A Burst Modulation/Demodulation Method for Short-packet Wireless Communication Systems

Takafumi FUJITA, Daisei UCHIDA, Yosuke FUJINO, Osamu Kagami, and Kazuji WATANABE
NTT Network Innovation Laboratories, NTT Corporation
1-1 Hikari-no-oka, Yokosuka-shi, Kanagawa 239-0847, Japan
E-mail: fujita.takafumi@lab.ntt.co.jp

***Abstract*— This paper presents a burst modulation /demodulation method for narrowband wireless communication systems, whose traffic is especially dominated by short packet bursts. In order to improve transmission efficiency and burst synchronization performance, the proposed method provides a preamble-less frame structure with minimum number of training symbols. This paper also presents the experimentally measured performance of hardware prototypes of the proposed modulator and demodulator. The basic operation and practical performance are confirmed through testbed studies.**

Index Terms— burst modem, ubiquitous, transmission efficiency, burst synchronization, testbed study.

I. INTRODUCTION

The idea of "interconnection of intelligent objects" was proposed in the TRON project by K. Sakamura [1], and "ubiquitous computing" was raised by M. Weiser [2]. The improvements in electronics and information technologies enable these "ubiquitous" concepts to become achievable targets. Diversified services such as tele-metering, security, logistics, and disaster prevention are expected to appear by interconnecting small devices such as sensors or radio-frequency identifications (RF-IDs). Here, the Wide Area Ubiquitous Network seems one of the potential infrastructures [3]. In the Wide Area Ubiquitous Network, wide-area accessibility and cost-effectiveness are the most basic requirements. With respect to achieving wide-area accessibility, cellular systems such as IMT-2000 are promising candidates. However, they are not suitable for cost-sensitive applications like RF-ID services, because it is uneconomical to afford a huge number of wireless terminals. Although current RF-IDs or sensor-networks are cost-effective, they sometimes suffer access restrictions such as blind zones. In the Wide Area Ubiquitous Network, these problems are solved by its reduced number of base stations and long distance transmission capability. In addition, we have studied and reported its feasibility as determined by field experiments [3]. It was confirmed that 5-kilometer wireless transmission with 10 dBm transmission power is achievable with a narrowband wireless system design.

In these systems, supporting short-packet traffic with high transmission efficiency becomes essential, because tele-metering for utility bills or inventory management of logistics does not always require broad bandwidth per device, but total cumulated volume is high in uplink connection. Thus, it is desirable to reduce the number of training symbols as much as possible, because they severely deteriorate transmission efficiency. Moreover, in order to achieve long transmission distances, demodulation performance is essential in low carrier-to-noise power ratio (CNR) environments. Fading durability should be also guaranteed for mobility management.

In order to meet these requirements, this paper proposes a frame structure and a synchronization method that suit short-packet modulation/demodulation [4]. In the proposed method, successive training symbols are eliminated to improve transmission efficiency, whereas a minimum number of scattered pilot symbols are reserved for precise burst synchronization. They enable coherent-detection demodulators to achieve symbol timing recovery, slot synchronization, carrier frequency correction and channel tracking in low CNR environments. At last, the proposed method is implemented as a hardware prototype and experiments confirm their basic operation and performance.

The rest of this paper is organized as follows. Section II introduces the system target and requirements. Section III overviews the conventional methods and Section IV explains our proposed method. Section V covers the experimental studies. Finally, Section VI presents our conclusions.

II. SYSTEM TARGET

In order to support a huge number of wireless terminals and flexible frame structuring, burst communication with time division multiple access (TDMA) is most suitable. The modulator/demodulator specifications of the target system are shown in Table 1. We assume a quite narrow signal bandwidth like pager systems. In order to achieve superior spectral efficiency, quaternary phase shift keying (QPSK) is adopted. Forward error correction (FEC) technique is also indispensable for long distance transmission and mitigation of fading effect. Minimum data packet size is assumed to be about 128 bits (ID information size mentioned in [5]), and variations up to 128 bytes considering more complex applications. Here, in order to transmit 128 bits of data after FEC coding, for example, the burst length becomes about 150 symbols. Because the required energy-per-symbol to noise-power-density (E_s/N_0) for a practical bit error rate (BER) after FEC is around 3~4 dB, the CNR required for not only signal detection but also burst synchronization is a very challenging target.

III. CONVENTIONAL METHOD

Training symbols such as preamble or midamble are generally used for burst synchronization. The conventional training symbol arrangements are shown in Fig. 1(a) and (b), respectively. With the conventional methods, each burst requires relatively long successive training sequences for burst synchronization, which severely degrades transmission efficiency. Moreover, they also face another difficulty for our target. Because we assume low symbol-rate systems, the transmission performance is severely degrades in time-varying channels. Thus, a channel tracking

technique such as pilot-symbol assisted modulation [6] should be applied, even if it might cause transmission efficiency degradation.

IV. PROPOSED METHOD

A. Configuration

In order to solve the presented problems, we set a small number of training symbols in the frame structure and use them also for all burst synchronization processes. The proposed burst frame structure is shown in Fig. 2. Burst synchronization is realized by both the data symbols and the scattered training symbols. Transmission efficiency is improved by eliminating successive training symbols. The proposed training symbols are not only used for pilot-symbol assisted demodulation, but also for improving slot synchronization performance. With the proposed frame structure, we achieve transmission efficiencies better than 85% regardless of frame burst length [4].

A block diagram of the modulator is shown in Fig. 3. Convolutionally encoded data are interleaved and multiplexed with encoded pilot patterns. After symbol mapping, burst signals are filtered and upconverted into intermediate-frequency (IF) signals. Next, a block diagram of the demodulator is shown in Fig. 4. Burst synchronization is established in four steps: symbol timing recovery, slot synchronization, carrier frequency correction and channel tracking. At first, the received burst signals are stored in burst memory. Next, symbol timing is recovered from the envelope information of the entire burst. Slot synchronization and carrier frequency correction are then simultaneously carried out by using the output of the correlation calculation. Finally, residual carrier frequency offset and channel variations are removed by using the scattered coded pilots.

B. Scattered coded pilots

In order to achieve accurate slot synchronization with the limited number of training symbols, pilot patterns should be properly scattered and encoded in the modulator. This encoding allows us to achieve not only frame detection but also carrier frequency offset estimation. The pilot patterns are generated by an orthogonal codeset such as Walsh-Hadamard matrix **V**. **V** is given by

$$\mathbf{V} = \begin{pmatrix} \mathbf{v}_1 \\ \mathbf{v}_2 \\ \vdots \\ \mathbf{v}_{N_p} \end{pmatrix} = \begin{pmatrix} v_{1,1} & v_{1,2} & \cdots & v_{1,N_q-1} \\ v_{2,1} & v_{2,2} & \cdots & v_{2,N_q-1} \\ \vdots & \vdots & \ddots & \vdots \\ v_{N_p,1} & v_{N_p,2} & \cdots & v_{N_p,N_q-1} \end{pmatrix} \quad (1)$$

where N_p is the number of symbols for each pilot; N_q is the number of pilots in a burst. Note that the $\mathbf{v}_m$ codesets are orthogonal to each other. Next, an encoded pilot pattern matrix **U** is generated by encoding matrix **V** differentially in the column direction. **U** is given by

$$\mathbf{U} = \begin{pmatrix} \mathbf{u}_1 \\ \mathbf{u}_2 \\ \vdots \\ \mathbf{u}_{N_p} \end{pmatrix} = \begin{pmatrix} u_{1,1} & u_{1,2} & \cdots & u_{1,N_q-1} & u_{1,N_q} \\ u_{2,1} & u_{2,2} & \cdots & u_{2,N_q-1} & u_{2,N_q} \\ \vdots & \vdots & \ddots & \vdots & \vdots \\ u_{N_p,1} & u_{N_p,2} & \cdots & u_{N_p,N_q-1} & u_{N_p,N_q} \end{pmatrix} \quad (2)$$

where

$$u_{m,n+1} = u_{m,n} \times v_{m,n} \qquad \left(1 \le m \le N_p,\ 1 \le n \le N_q - 1\right). \quad (3)$$

The matrix elements of **U** are multiplexed into a burst and transmitted according to the arrangement in Fig. 2. Note that the orthogonal codesets are differentially encoded with (N_p+N_d) symbol spacing, where N_d is the data length between adjacent pilots. This technique enables us to achieve precise slot synchronization and carrier frequency correction.

C. Symbol timing recovery

In the proposed demodulator configuration, symbol timing is recovered before any other synchronization steps. Thus, the symbol timing recovery must offer superior durability against carrier frequency offset and varying channel status. The symbol timing is detected from low sampling-rate burst signals using discrete Fourier transform (DFT) [7]. DFT output is given by

$$E = \sum_{l=1}^{n_s\left((N_q-1)(N_p+N_d)+N_p\right)} \left|r(t_l)\right|^2 \cdot \exp\left(\frac{-j2\pi f_s t_l}{n_s}\right) \quad (4)$$

where n_s denotes an over-sampling factor against symbol time; $r(t_l)$ denotes the over-sampled received signals after the pulse-shaping; t_l denotes the sample-by-sample index in the time domain. Symbol timing phase θ is then given by

$$\theta = \tan^{-1}\frac{\mathrm{Im}[E]}{\mathrm{Re}[E]}. \quad (5)$$

According to detected symbol timing phase θ, the coefficient of the FIR filter is updated and adequate burst signals are output. Because DFT is applied to the envelope, the effects of carrier frequency offset and varying channel status can be avoided.

D. Slot synchronization

In the proposed demodulator, slot synchronization is achieved by the complex correlation of the scattered coded pilots. As mentioned in symbol timing recovery, durability against carrier frequency offset is essential, because it cannot be ignored with low symbol-rate narrowband systems.

A block diagram of the frame detector and carrier frequency offset estimator is shown in Fig. 5. For detecting the frame, the differentially-detected signals with (N_p+N_d) symbol spacing are used for evaluating the correlation. The differentially-detected symbol is given by

$$c(t_k) = s(t_k)^* \times s\left(t_{k+(N_p+N_d)}\right) \quad (6)$$

where $s(t_k)$ denotes the received symbol after symbol timing recovery; t_k denotes the symbol-by-symbol index in the time domain within narrow aperture window; * represents the complex conjugate. Here, differentially-detected matrix $\mathbf{W}(t_k)$ and vectors $\mathbf{w}_m(t_k)$ can be defined using Eq.(6). $\mathbf{W}(t_k)$ and $\mathbf{w}_m(t_k)$ are given as

$$\mathbf{W}(t_k) = \begin{pmatrix} \mathbf{w}_1(t_k) \\ \mathbf{w}_2(t_k) \\ \vdots \\ \mathbf{w}_{N_p}(t_k) \end{pmatrix} = \begin{pmatrix} w_{1,1} & w_{1,2} & \cdots & w_{1,N_q-1} \\ w_{2,1} & w_{2,2} & \cdots & w_{2,N_q-1} \\ \vdots & \vdots & \ddots & \vdots \\ w_{N_p,1} & w_{N_p,2} & \cdots & w_{N_p,N_q-1} \end{pmatrix} \quad (7)$$

$$w_{m,n} = c\left(t_{k+(m-1)+(n-1)(N_p+N_d)}\right). \quad (8)$$

Frame detection is carried out by calculating the cross-correlation between **V** and $\mathbf{W}(t_k)$. Frame beginning index $t_{K\max}$ is finally detected as

$$t_{K_{\max}} = \arg\max_{t_k} \left| C_{cross}(t_k) \right| \quad (9)$$

where total cross-correlation $C_{cross}(t_k)$ is given by

$$C_{cross}(t_k) = \sum_{m=1}^{N_p} \mathbf{v}_m^* \cdot \mathbf{w}_m(t_k). \quad (10)$$

We can obtain the peak correlation timing as the slot timing within the aperture window of slots. Here, note that $\mathbf{v_m} \cdot \mathbf{w_m}(t_k)$ are likely to be orthogonal because of Walsh-code orthogonality with adjacent timing (e.g. $t_k = t_{K\max} \pm 1$). Thus, we can expect finely resolved peaks. Also note that the correlation is not degraded by carrier frequency offset, because $\mathbf{w_m}(t_k)$ represents differentially not coherently detected signals. Thus, we can realize accurate slot synchronization with just a few training symbols.

The frame miss-detection rate performance against E_s/N_0 in AWGN is shown in Fig. 6. The performances with the conventional methods are also shown for reference. As shown in Fig. 6, frame miss-detection rate performance improves with increasing burst size, simply because the number of scattered coded pilots increases. According to Fig. 6(a), it is shown that a similar number of training symbols achieves comparative frame miss-detection rate performance in the AWGN environment. With the shortest burst size (148 symbols), required E_s/N_0 for the frame miss-detection rate = 10^{-2} is smaller than 3 dB, which seems satisfactory performance considering required E_s/N_0 for frame error rate (FER) of 10^{-2} with 16 byte packets is about 3 dB. On the other hand, as shown in Fig. 6(b), the proposed method significantly improves the performance in fading environments. With respect to required E_s/N_0 for frame miss-detection rate of 10^{-2}, that of the proposed method with N_T=20 is better than that of the conventional one with N_T=16, and comparable to that of the conventional one even with N_T=32, where N_T denotes the number of training symbols in the burst. This is because the proposed method utilizes the pilots scattered over the whole burst, which can offset the impact of fading.

E. Carrier frequency correction

The calculated correlation in the frame detector $C_{cross}(t_{K\max})$ (see Eq.(9) and Eq.(10)) represents not only the cross-correlation with the proposed scattered coded pilots, but also auto-correlation with (N_p+N_d) symbol spacing. Thus, as shown in [8], the carrier frequency can be estimated from $C_{cross}(t_{K\max})$. The estimated frequency offset is given by

$$\hat{f}_{off} = f_s \times \frac{1}{2\pi(N_p + N_d)} \times \tan^{-1} \frac{\mathrm{Im}\left[C_{cross}(t_{K_{\max}})\right]}{\mathrm{Re}\left[C_{cross}(t_{K_{\max}})\right]}. \quad (11)$$

The received symbol sequence after carrier frequency correction is given by

$$s'(t_k) = s(t_k) \times \exp\left(-j2\pi \hat{f}_{off}(t_k - t_0)\right) \quad (12)$$

where t_0 denotes an arbitrary time constant. According to Eq.(11), the pull-in range of carrier frequency correction depends on the symbol spacing of scattered coded pilots: N_p+N_d. Thus, we can mitigate frequency sensitivity by replacing Eq.(11) with

$$\hat{f}_{off}{}' = f_s \times \frac{1}{2\pi(N_p + N_d)} \times \left(\tan^{-1} \frac{\mathrm{Im}\left[C_{cross}(t_{K_{\max}})\right]}{\mathrm{Re}\left[C_{cross}(t_{K_{\max}})\right]} + a \right) \quad (13)$$

$$(a = 0, \pm 2\pi, \pm 4\pi, \cdots)$$

where a denotes a search parameter that considers phase slipping in carrier frequency offset estimation. Valid a can be selected according to the result of cyclic redundancy check (CRC).

The frame miss-detection rate against normalized carrier frequency offset is shown in Fig. 7. Here, the carrier frequency offset f_{off} is normalized by symbol modulation rate f_s. It is shown that the frame miss-detection rate achieves superior flat pull-in performance independent of the carrier frequency offset, because symbol timing recovery and slot synchronization are not affected by carrier frequency offset. In Fig. 7, FER performances with various parameter a values are also shown. According to Fig. 7, the pull-in range of the carrier frequency correction is about $\pm 0.012 f_s$, while the expected range is $\pm 0.014 f_s$ (see Eq.(11)). The oscillator instability requirement sometimes becomes severe depending on the carrier frequency, however, this problem can be solved by increasing the number of search parameter a.

F. Channel tracking

With the conventional frame structure shown in Fig. 1(a) and (b), it is difficult to track time-varying channels. With the proposed frame structure, on the other hand, residual carrier frequency offset and channel variations can be compensated by pilot-symbol assisted modulation [6].

In order to improve the signal-to-noise power ratio (SNR) property at each pilot position, multiple pilot symbols are utilized for each channel estimation. The burst signals are demultiplexed into pilot and data symbols. The averaged channel response for each n-th pilot position is given by

$$h_{pilot}(p_n) = \frac{1}{N_p} \sum_{m=1}^{N_p} u_{m,n}^* \times s'(t_k) \left(1 \le n \le N_q\right), \quad (15)$$

which is accompanied with pilot decoding. Finally, the channel response of the n-th data payload positions can be linearly interpolated from $h_{pilot}(p_n)$ and $h_{pilot}(p_{n+1})$.

G. Overall performances

The FER performance versus E_s/N_0 in Doppler and quasi-static Rayleigh fading channels with 16 byte bursts is shown in Fig. 8. The performances of the conventional methods are shown for reference. In quasi-static channels, conventional methods achieve slightly better performance than the proposed one, because they can utilize more total energy of the training symbols for channel estimation. On the other hand, in time-variant Doppler channels, the proposed method lowers the required E_s/N_0 for the FER of 10^{-2} by about 4 dB compared to quasi-static channels, whereas conventional methods suffer from irreducible errors. There are two reasons for this. One is the performance improvement in frame miss-detection rate, which is caused by effective utilization of the whole scattered training symbols (see Fig. 6(b)). The other is the channel tracking capability, which is not offered by the conventional methods. Here, note that the proposed method achieves 6 % better transmission efficiency than the conventional methods. Thus, the proposed methods is advantageous both in transmission efficiency and burst synchronization performance.

V. Experimental Evaluation

The proposed method is implemented as a hardware prototype for testbed studies. The module was configured with field-

programmable-gate-array (FPGAs) and digital-signal-processor (DSPs), and its FER performance was measured. Radio-frequency modules were connected in series and the transmitter and receiver were linked via a fading simulator. Experimental parameters are shown in Table 2. We assumed AWGN and a flat Rayleigh fading channel. Doppler frequency was set considering the typical speeds of vehicles in residential areas. The measured overall FER performance against E_s/N_0 is shown in Fig. 9. The experimental performances well match the computer-simulated results. Thus, the basic operation and performance of the proposed method are confirmed by the testbed studies.

VI. CONCLUSIONS

This paper presented a burst synchronization method that suits short-packet wireless communications with narrowband signal bandwidth. The preamble-less frame structure improves transmission efficiency, and the proposed burst synchronization method enables robust operation against carrier frequency offset and varying channel status in low CNR environments. Furthermore, the testbed studies of the hardware prototype confirmed its basic operation and performance. It is clarified that the proposed method is sufficiently practical for short-packet wireless communication systems.

REFERENCES

[1] K. Sakamura, "The Tron Project," *IEEE Micro*, vol.7, no.2, pp.8-14, April 1987.

[2] M. Weiser, "Some computer science issues in ubiquitous computing," *Communications of the ACM*, vol.36, no.7, pp.75-84, July 1993.

[3] M. Umehira, H. Saito, O. Kagami, T. Fujita, and Y. Fujino, "Concept and Feasibility Study of Wide Area Ubiquitous Network for Sensors and Actuators," *in Proc. IEEE VTC-Spring 2007*, May 2006.

[4] T. Fujita, D. Uchida, Y. Fujino, O. Kagami, and K. Watanabe, "A Short-burst Synchronization Method for Narrowband Wireless Communication Systems," *in Proc. IEEE ISWPC2007*, Feb. 2007.

[5] ISO/IEC Std.: "Identification Cards – Contactless integrated circuit(s) cards –vicinity cards–," 2001.

[6] J. K. Cavers, "An analysis of pilot symbol assisted modulation for Rayleigh fading channels," *IEEE Trans. Vech. Tech.*, vol.40, no.4, Nov. 1991.

[7] Y. Matsumoto, M. Morikura, and S. Kato, "A burst Mode All-Digital High Speed Clock Recovery Circuit –Block Clock Recovery Scheme–," *IEICE Trans. Commun.*, vol.J75-B-II, no.6, pp.354-362, Jun. 1992.

[8] M. Luise, and R. Reggiannini, "Carrier frequency recovery in all-digital modems for burst-mode transmissions," *IEEE Trans. Commun.*, vol.43, no.2/3/4, Feb./Mar./Apr. 1995.

Table 1 Modulator/demodulator specifications.

Modulation method	π/4-QPSK
Modulation rate	9,600 symbol/s
Pulse-shaping filter	Root cosine roll-off filter (Roll-off factor=0.5)
Signal bandwidth	14.4kHz
Forward error correction	Convolutional encoding, Viterbi decoding (k=7, r=1/2)
Interleave depth	16 bits
Burst data length	16, 32, 64, 128 bytes

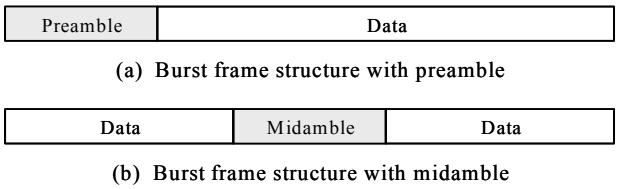

Fig. 1 Conventional burst frame structures.

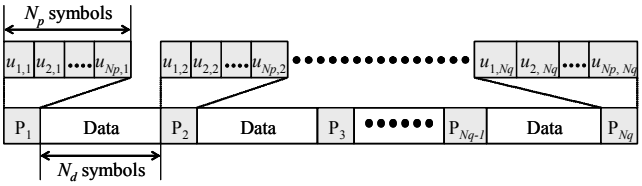

Fig. 2 Proposed burst frame structure.

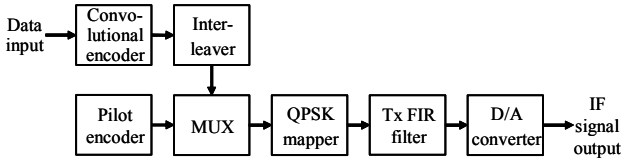

Fig. 3 Modulator.

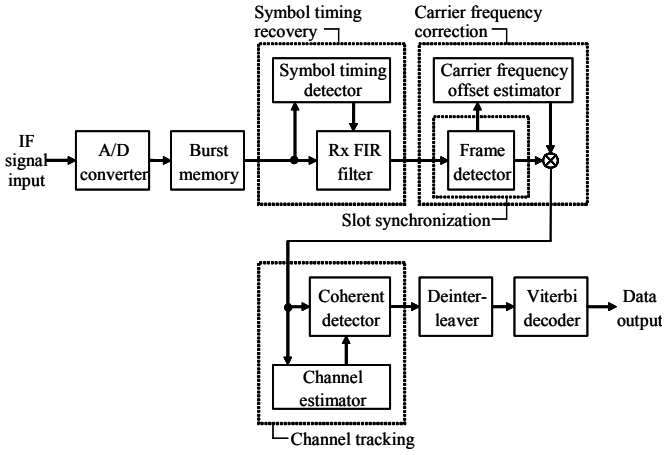

Fig. 4 Demodulator.

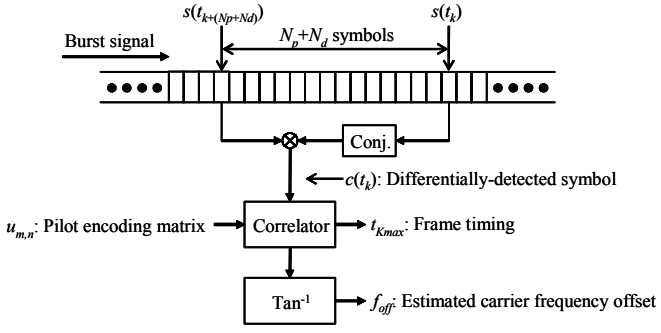

Fig. 5 Frame detector and carrier frequency offset estimator.

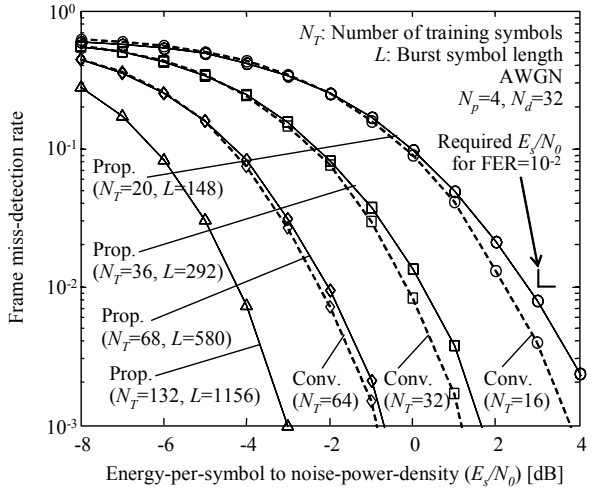

(a) AWGN

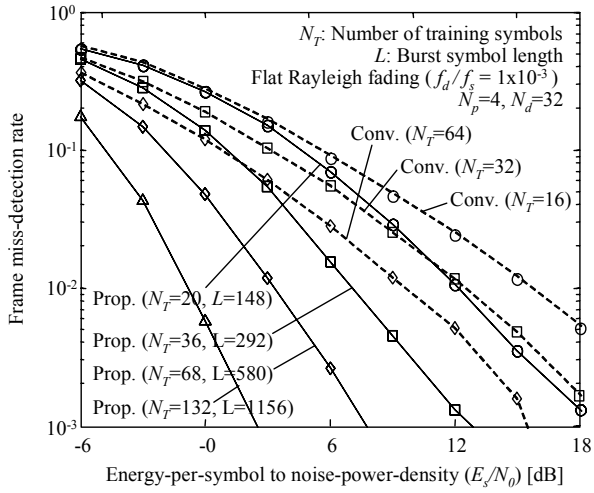

(b) Fading

Fig. 6 Frame miss-detection rate performance vs. energy-per-symbol to noise-power density.

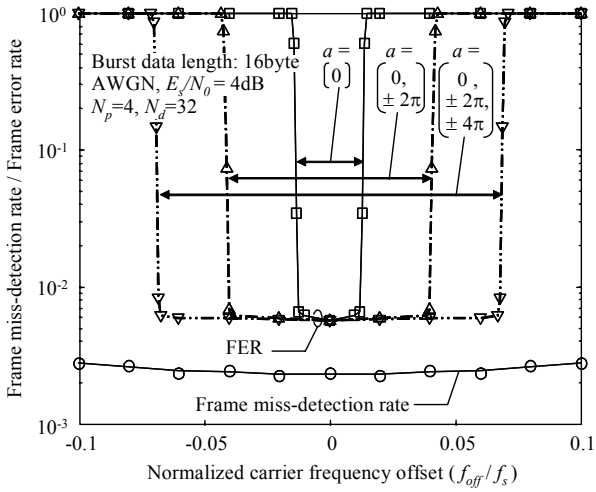

Fig. 7 Frame miss-detection rate and frame error rate performance vs. normalized carrier frequency offset.

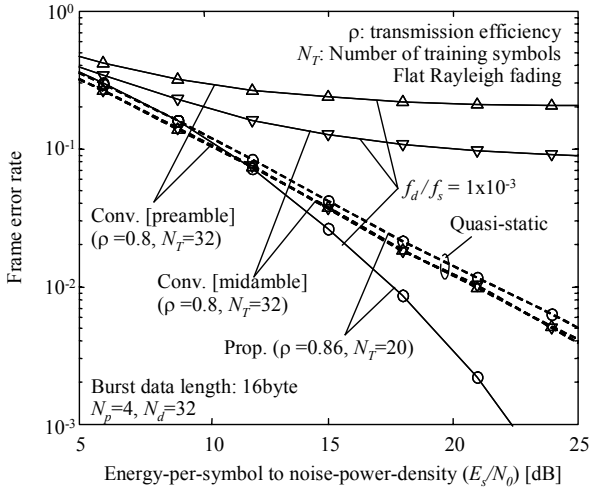

Fig. 8 Frame error rate performance vs. energy-per-symbol to noise-power-density in Doppler and quasi-static fading channels.

Table 2 Experimental parameters.

Propagation channel	AWGN / Flat Rayleigh fading
Doppler frequency	10 Hz (mobile speed: 40km/h)
Carrier frequency	286 MHz
Cyclic redundancy check	16 bits
Data transmission rate	9,600 bit/s
Data burst length	16 bytes
Burst length	148 symbols (N_p=4, N_d=32)

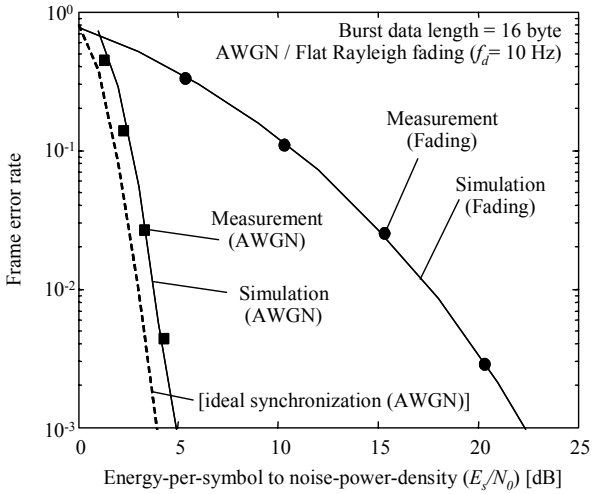

Fig. 9 Experimentally measured frame error rate performance vs. energy-per-symbol to noise-power density.